A Novel Lyapunov-Based Nonlinear Controller Design for Model-Based MPPT of the Thermoelectric Generators

Sarah Kowsari Mogadam[1], Mahdi Salimi[*2], Seyyed Mohammad Taghi Bathaee[3], Davar Mirabasi[1]

1- Department of Electrical Engineering, Ardabil Branch, Islamic Azad University, Ardabil, Iran

2- Faculty of Engineering and Science, University of Greenwich, Kent, ME4 4TB, UK

3- Faculty of Electronic & Computer Engineering, K.N.Toosi University of Technology, Tehran, Iran

Abstract: A novel model-based approach for closed-loop control and maximum power point(MPP) tracking of thermoelectric generators (TEG) has been presented using the nonlinear Lyapunov-based approach. As the TEG power derivative is always zero at MPP, it can be employed as a feedback signal for the controller. Hence, the reference value of controller will always be zero which simplifies the controller structure significantly. Since the reference calculation block can be removed, there is no need for a cascade multi-loop controller which can improve the controller's dynamic response. Due to the elimination of reference calculation unit, the proposed controller demonstrates superior performance, e.g., during temperature and load changes. The asymptotic stability of proposed controller has been proved. To evaluate the accuracy of the controller, it is simulated by using MATLAB software. Moreover, the experimental responses are provided by employing the TMS320F28335 DSP from *Texas Instruments*. According to the simulation and experimental results and despite temperature and load changes in a wide range, the closed-loop system shows a stable and robust performance

as well as fast dynamic response and zero steady-state error. Finally, the response of the proposed controller is at least two times faster than the P&O controller.

Keyword:

Thermoelectric Generator, Asymptotic Stability, Nonlinear Controller, Lyapunov-Based Controller, Load and Temperature Change

1- Introduction

Due to shortage of the fossil fuels as well as the environmental pollution caused by their use for electricity generation, the employment of renewable energy resources e.g. wind, photovoltaic and thermoelectric power plants has increased sharply in recent years [1,2]. However, considering the high capital cost of renewable systems and their poor power efficiency, the optimal and efficient use of these energy generators is vital. For instance, it is well known that the operating point of a photovoltaic system should be monitored and updated continuously to meet the maximum power point (MPP) requirements against load and environmental conditions changes. Similar to photovoltaic panels, a thermoelectric generator (TEG) can be classified as a renewable energy source since it can be used for waste energy harvesting in different applications e.g. hybrid electric vehicles [3]. Also, the TEG system has a DC output characteristic and the output power significantly depends on the operating point. It should be noted that one of the main issues in the utilization of TEG systems is the MPP changes with the temperature of heat source [4]. For this reason, the operating point of TEG must be continuously adjusted to

guarantee MPP operation [5]. To achieve the mentioned goal, a DC-DC converter can be employed as an interface between a TEG and an electric load. So, TEG maximum power point tracking (MPPT) can be performed by proper adjustment of the converter duty cycle. For example, Arora proposed the application of a buck DC-DC converter for MPPT of TEGs [6]. Considering the maximum power transfer theorem, if the load and TEG internal resistances be equal, the maximum power will be generated by the input source. Due to the uncertain nature of the load value, a DC-DC converter is employed between the load and source to match the equivalent input resistance of converter with the TEG resistance. Hence, the real-time values of load and internal resistances are needed for the implementation of mention open-loop controller. As a result, additional voltage and current sensors are required which increases the implementation cost. Finally, the use of an open-loop controller can result in a steady-state error due to unmodeled elements e.g. parasitic resistances. Basically, it is possible to track the MPP of TEG source using all DC-DC and DC/AC converters. However, the application of boost chopper converters is more promising due to the non-pulsating waveform and lower ripple of input current [7]. In the buck DC-DC converter, the input power source is connected in series with the main switch. Hence, the TEG current will be pulsating indeed and it is not possible to stabilize the converter operating point without the use of heavy LC filters at the input port of converter.

In the literature, several closed-loop controllers for MPPT of renewable energy systems have been reported. Regarding the performance of MPPT method, a comprehensive comparison is provided based on design complexity, the number of required sensors, implementation cost, dynamic response, stability, tracking accuracy, and grid connection capability [8]. Among the mentioned approaches, perturb and observe (P&O) [9,10] and hill-climbing [11] methods are more popular due to the simplicity of implementation and acceptable steady-state and dynamic responses, especially in industrial applications. In the P&O method, the output power of TEG source is perturbed at first. Then, the TEG power is measured at the new operating point once the transient response is settled. Considering the initial perturbation and power changes, the direction of next perturbation can be realized [12]. If the operating point of converter is perturbed by the duty cycle changes, the MPPT technique is called hill-climbing [13]. In both P&O and hill-climbing, the perturbation amplitude and frequency should be selected in a way that meets the steady-state and dynamic requirements. The smaller perturbation amplitude can result in a smaller steady-state oscillation and energy loss [14]. On the other hand, to improve the dynamic response (especially for mobile loads), the perturbation amplitude (step size) should be large enough to meet the load requirements. As long as the response of previous perturbation isn’t settled, the controller isn’t allowed to apply the next perturbations. This issue can deteriorate the controller's dynamic response. In traditional P&O, a fixed-amplitude perturbation is used in a way that satisfies both the

steady-state and dynamic response. Superior performance can be achieved by employing the two-phase P&O [15] which uses different step sizes during steady-state and transient conditions. It can improve the dynamic response speed and reduce steady-state oscillations. In addition, the adaptive P&O methods have been reported for an efficient selection of step sizes which can effectively improve the performance of traditional P&O algorithms. However, since the P&O used the oscillations for discovering the next possible changes at MPP, even the adaptive approaches cannot remove the steady-state oscillations completely.

Yahya and Alomari [4] proposed a Kalman filter-based MPPT approach for the TEG systems. Considering the valid range of duty cycle i.e. $0.1 \leq D \leq 0.9$, the TEG output power is measured for minimum and maximum duty cycles. Then, by analysing the direction of power changes between two adjacent points, the range of duty cycle is limited gradually to achieve the MPP. Considering the wide changes in the duty cycle between maximum and minimum valid values, the controller might have an oscillatory response at the beginning of tracking. Moreover, the response settling time can be too large which deteriorates the dynamic response of MPPT controller.

To solve the associated disadvantages of P&O and hill-climbing methods, the utilization of intelligent controllers such as neural networks [16] has been reported for MPPT of thermoelectric systems [17].

Also, to cope with the non-uniform temperature distribution problem which can result in the multiple local MPPs, an adaptive neural optimization technique for MPPT of the TEGs has been employed. The adaptive neural network can efficiently and rapidly seek the global MPP using the generalized regression which performs a suitable mapping between the TEG output power and duty cycle of a boost DC-DC converter. However, during the neural network training phase, an adequate amount of sample data for different operational conditions is needed. More importantly, the electric characteristics of an industrial TEG module e.g. open-circuit voltage and internal resistance may differ considerably, even for TEGs with identical part numbers [18]. Hence, specific data should be generated over a long period and employed during the learning phase of each case separately which can be an expensive and time-consuming task.

In addition to intelligent methods, the application of modern optimization techniques e.g. grey wolf, and cuckoo search algorithms for the MPPT of renewable energy sources has gained more attention in recent years. The major advantages are superior convergence speed and robustness against the local maximums. Also, the controller parameter tunning isn't required which facilitates the design process. Adeel Feroz et.al reviewed and compared the MPPT of TEG-Photovoltaic(PV) system with optimization techniques under various non-static modes [19]. Due to the nonlinear behaviour of combined renewable TEG-PV systems, the classical optimization approaches e.g. particle swarm optimization might fail in a wide range of changes. However, modern

optimization techniques suffer from complex calculations and higher implementation costs [20].

According to the drawbacks of mentioned methods, the use of model-based approaches has been further studied in recent years [21]. The advantages of model-based MPPT controller are better stability and robustness and superior dynamic steady-state responses. The design process begins with the calculation of controller's reference signal for MPPT. Then, a model-based controller e.g. linear, adaptive, predictive, and robust is employed for the voltage/current control of renewable power sources. For example, Sudwilai designed a linear controller for MPPT of PV systems [22]. However, linear controllers are designed based on small-signal approximation and system linearization around the operating point [23]. For this reason, despite the simplicity of linear controller design, the closed-loop stability over a wide range of environmental condition changes cannot be guaranteed, considering the nonlinear model of the DC-DC converter [24]. Hence, in recent years, the application of nonlinear controllers for the MPPT of PV and TEG systems has gained more attention. Since the exact model of closed-loop system is used for nonlinear controller design, the stability hasn't been adversely affected by wide changes in the operating point. Among the nonlinear controllers, the sliding mode control (SMC) [25,26] and adaptive control [27,28] are more popular. The SMC has been widely employed for the closed-loop control of power electronics converters due to its robust behaviour, fast dynamic response, and ease of practical

implementation. It is designed in a way that forces the response of controller toward a sliding surface. Considering the switching nature of control effort in SMC, very high-frequency pulse gates can be applied to the converter which will deteriorate the converter power efficiency and might result in the failure of semiconductor switches. To limit the switching frequency range and reduce the chattering, the application of a terminal sliding mode controller has been reported for MPPT of TEG [29]. It employs a nonlinear combination of error variables in the sliding surface which can reduce chattering. The controller has a faster dynamic response compared to the standard P&O method. However, the design considerations of SMC e.g. hitting, stability, and existence conditions are not analyzed thoroughly in the recent reference. As a result, the controller robustness cannot be guaranteed in a wide range of changes.

To cope with the mentioned drawbacks and improve the stabilization of MPPT controllers, a novel nonlinear single-loop controller is presented in this paper, which is designed based on the Lyapunov stability. The controller generates the duty cycle of boost DC-DC converter using the TEG power derivative as a feedback signal. It should be noted that the time derivative of TEG power is always zero at MPP. Hence, if the output power derivative is employed as a feedback signal, the reference value will be zero which simplifies the controller structure significantly. Since the reference calculation block can be removed, there is no need for a cascade multi-loop controller and as a result, the controller dynamic response can be improved. Due to the elimination

of reference calculation unit, the proposed controller enjoys a superior performance indeed e.g., during temperature and load changes. The asymptotic stability of proposed controller is proved using the Lyapunov stability theorem and Barbalat lemma. The calculated duty cycle as the controller output is applied through a PWM unit and driver circuit to the converter switch. Hence, the switching of the converter will be fixed, regardless of the operating point changes. To evaluate the accuracy and efficiency of the proposed approach, it is simulated by using MATLAB software. Moreover, the experimental responses are provided by employing the TMS320F28335 digital signal processor from *Texas Instruments*.

The methodology of research is as follows. First, the comprehensive model of the whole system is extracted by state-space modelling of the DC-DC converters and using the electric model of the TEG system. Then a fixed-frequency nonlinear controller is developed to stabilize the closed-loop system using the Lyapunov controller. Also, the asymptotic stability of the proposed nonlinear controller is proved analytically within the whole operational range of the system. Finally, using the PC-based simulations and experimental results, the effectiveness and accuracy of the controller are verified in comparison with the standard P&O controllers.

2- System modelling

In this section, the electric model and MPP operation of TEG system are reviewed. Also, the averaged state-space model of the boost DC-DC converter which can be employed for MPP tracking of the TEG power source will be presented.

2-1 TEG modelling

It is well-known that thermoelectric generators can be modelled as a DC voltage source (V_{OC}, open-circuit voltage) in series with an internal resistor (R_{TEG}) which is illustrated in Fig.1 [30]. The value of V_{OC} depends on the temperature difference ($\triangle T$) between the hot and cold sides of TEG:

$$V_{OC} = \alpha \triangle T \qquad (1)$$

where α is the Seebeck coefficient. The values of R_{TEG} and α may slightly change with temperature. However, this issue doesn't deteriorate the performance of proposed controller, as these parameters aren't present in the developed control law. This will be explained in the next sections in more detail.

In Fig.2, the current-voltage (I-V) and power-voltage (P-V) characteristics of a typical TEG for different temperature differences are illustrated [30]. According to the TEG model in Fig.1, the output voltage can be written as follows which explains the linear I-V characteristic of TEG.

$$V_{TEG} = V_{OC} - R_{TEG} I_{TEG} \quad (2)$$

or:

$$I_{TEG} = -\frac{1}{R_{TEG}} V_{TEG} + \frac{V_{OC}}{R_{TEG}} \quad (3)$$

and P-V curve can be simplified as:

$$P_{TEG} = I_{TEG} V_{TEG} = -\frac{1}{R_{TEG}} V^2{}_{TEG} + \frac{V_{OC}}{R_{TEG}} V_{TEG} \quad (4)$$

The value of external load (R_L) determines the operating point of TEG, as illustrated in Fig.3.

According to the maximum power transfer theory, the output power (P_{TEG}) will be maximum if the $R_L = R_{TEG}$ is satisfied. Hence, the voltage and current of TEG at MPP can be written as:

$$I_{TEG} = \frac{V_{OC}}{R_L + R_{TEG}} = \frac{V_{OC}}{2R_{TEG}} \quad (5)$$

$$V_{TEG} = \frac{R_L}{R_L + R_{TEG}} V_{OC} = \frac{V_{OC}}{2} \quad (6)$$

2-2 Dynamic modelling of boost DC-DC converter:

The power topology of boost DC-DC converter which is employed for MPPT of TEG, is shown in Fig.4. In the conventional approaches, a capacitive filter is generally needed which facilitates the controller design through the fast dynamics removal. On the other hand, due to the application of Lyapunov-based nonlinear controller - which can ensure the stability of system in a wide range of ambient temperature changes - the input capacitor isn't used in this paper. In this case, the current of an inductor and TEG source will be identical which can simplify the controller. Input current ripple can be limited by the employment of wide bandgap semiconductor switches e.g. high-frequency GaN/SiC power switches. Also, a converter load is a battery which behaves as a DC voltage source. Considering the main objective of MPPT controller, the load doesn't play an important role in the input power dynamics. Considering the switching signal status in continuous conduction mode, the boost DC-DC converter can be modelled using the following sub-circuits.

Sub-circuit A) It is assumed that the power switch (S) is ON within $0 \le t \le t_{on}$ interval. Considering the structure of converter, it is clear that the diode is off in this switching status and the equivalent circuit of converter is shown in Fig.5-a. The state-space model of circuit in Fig.5-a can be written as follows:

$$\dot{x}_1 = \frac{1}{L} v_{TEG} \qquad (7)$$

where x_1 is the inductor current, v_{TEG} is the thermoelectric generator voltage and L is the inductor value.

Sub-circuit B) While the switching signal is low and the power switch (S) is OFF, the inductor current x_1 is directed toward the diode and turns it ON. In this switching interval, the equivalent circuit of converter is illustrated in Fig.5-b, and the state-space model of converter can be written as:

$$\dot{x}_1 = \frac{1}{L}(v_{TEG} - V_{Bat}) \qquad (8)$$

wherV_{Bat} e is the load voltage. Details of averaged state-space modelling for power electronics converters are presented in Appendix I. It should be noted that equation (7) describes the converter behaviour within $0 \le t \le t_{on}$ interval and equation (8) can be used in $t_{on} \le t \le T_s$ range. Defining $D = \frac{t_{on}}{T_s}$ as the switching duty cycle, equations (7) and (8) can be combined to generate the averaged state-space model of system by using (32)-(34) in Appendix I.

$$\dot{x}_1 = (\frac{1}{L} v_{TEG} - \frac{1-D}{L} V_{Bat}) \qquad (9)$$

The developed state-space model in equation (9) can be assumed as a start-point of nonlinear controller design for MPPT of TEG resources.

3- Controller design

3-1- Two-loop controller

The structure of two-loop controller for MPPT of TEG sources is shown in Fig.6 [31]. In this approach, the reference voltage (or current) of TEG at MPP is calculated in the outer loop, considering the real-time values of TEG voltage and current. Then by employing an inner loop which is responsible for input voltage (or current) control of the boost DC-DC converter, TEG output voltage (or current) is regulated at the reference value (V_{mpp} or I_{mpp}). By proper design of both inner and outer loops, the operation of the TEG source at MPP can be ensured. The inner loop can be implemented using conventional PI controllers. To improve the performance of inner loop in terms of stability and robustness, nonlinear controllers e.g. sliding mode, adaptive, and predictive approaches can be used. Regarding the inner loop design, the P&O method has widely been employed for reference value calculation. The main drawbacks of two-loop controllers for MPPT are:

1- Considering the application of two cascaded controllers, the mentioned structure cannot result in a fast dynamic response indeed. During the transient response of outer controller, the inner controller isn't able to track the MPP since the reference value isn't available.

2- Considering the nature of P&O approach, the reference signal, as well as the converter operating point, will be fluctuating around the MPP and the TEG power cannot be placed at the optimum operating point.

To cope with these issues, a novel single-loop controller is proposed for MPPT of TEG sources based on the power derivate of input source.

3-2 Lyapunov-based nonlinear controller design for MPPT of TEG

The state-space model of converter is given in equation (9). For the MPPT of a renewable energy source, a voltage (or current) closed-loop controller can be employed to push the operating point toward the MPP. In such an approach, the reference value of controller should be calculated accurately to ensure the operation of TEG at MPP. So, the closed-loop system will include two separate cascaded loops. The outer loop is responsible for reference signal calculation and the inner loop is employed for voltage (or current) regulation of the TEG source. However, the multi-loop controllers cannot result in a fast dynamic response. Moreover, the operating point of controller should be perturbed continuously to update the reference value during the TEG power profile changes. To cope with this issue, in this paper, the power derivative of TEG source is employed as the feedback signal of controller because the power derivative is always zero at MPP. So, an extra loop for the calculation of reference value is no longer needed and a single-loop controller can be used for MPPT. According to the power-voltage characteristic of a thermoelectric generator in Fig. 2, it is clear that the derivative of TEG power to voltage changes is always zero at MPP:

$$\left.\frac{dP_{TEG}}{dV_{TEG}}\right|_{MPP} = 0 \qquad (10)$$

As $\frac{dP_{TEG}}{dt}=\frac{dP_{TEG}}{dV_{TEG}}\times\frac{dV_{TEG}}{dt}$, it is seen that the time derivative of TEG power is zero at MPP as well.

$$\left.\frac{dP_{TEG}}{dt}\right|_{MPP}=0 \qquad (11)$$

According to (11), as the time-derivative of TEG power is zero at MPP, a Lyapunov-based nonlinear controller will be developed in this paper to force the feedback signal ($\frac{dP_{TEG}}{dt}$) into zero. The block diagram of proposed controller is illustrated in Fig.7.

To design the controller, an error variable of closed-loop controller can be defined as follows.

$$z=\left(\frac{dP_{TEG}}{dt}\right)_{ref}-\frac{dP_{TEG}}{dt}=0-\frac{dP_{TEG}}{dt}=-\frac{d}{dt}\left(v_{TEG}\times i_{TEG}\right) \qquad (12)$$

or:

$$z=-\frac{d}{dt}\left(v_{TEG}\times i_{TEG}\right)=-v_{TEG}\dot{x}_1-\dot{v}_{TEG}x_1 \qquad (13)$$

By placing the derivative of x_1 from equation (9) in (13):

$$z=-\frac{1}{L}v^2{}_{TEG}+\frac{1-D}{L}v_{TEG}V_{Bat}-\dot{v}_{TEG}x_1 \qquad (14)$$

Considering the time-derivative of equation (14), the dynamics of error variable can be written as.

$$\dot{z} = -\frac{2}{L} v_{TEG} \dot{v}_{TEG} - \frac{\dot{D}}{L} v_{TEG} V_{Bat} + \frac{1-D}{L} \dot{v}_{TEG} V_{Bat} - \ddot{v}_{TEG} x_1 - \dot{v}_{TEG} \dot{x}_1 \quad (15)$$

By combining equations (9) and (15):

$$\dot{z} = -\frac{2}{L} v_{TEG} \dot{v}_{TEG} - \frac{\dot{D}}{L} v_{TEG} V_{Bat} + \frac{1-D}{L} \dot{v}_{TEG} V_{Bat} - \ddot{v}_{TEG} x_1 - \frac{\dot{v}_{TEG}}{L} (v_{TEG} - (1-D) V_{Bat}) \quad (16)$$

To design the controller, the Lyapunov function of system can be assumed as follows:

$$V = \frac{1}{2} z^2 \quad (17)$$

In this case, the time-derivative of Lyapunov function is equal to:

$$\dot{V} = z\dot{z} \quad (18)$$

In equation (18), if it is assumed that:

$$\dot{z} = -cz \quad (19)$$

then the derivative of Lyapunov function will be:

$$\dot{V} = -cz^2 \quad (20)$$

where the scalar parameter *c* is a positive design coefficient.

By using equation (16), the time-derivative of Lyapunov function in equation (18) will be a semi-definite negative function which is presented in equation (20). Such an assumption results in the asymptotic stability of closed-loop system. Details of stability analysis are presented in Appendix II using the Barbalat lemma.

By substituting equations (14) and (16) into equation (19), the following equation can be obtained:

$$\ddot{v}_{TEG}x_1 + \dot{v}_{TEG}(cx_1 + \frac{3v_{TEG} - 2V_{Bat}}{L}) + \frac{c}{L}v_{TEG}(v_{TEG} - V_{Bat}) + (\dot{v}_{TEG}\frac{2V_{Bat}}{L} + cv_{TEG}\frac{V_{Bat}}{L})D + v_{TEG}\frac{V_{Bat}}{L}\dot{D} = 0 \quad (21)$$

where $\dot{v}_{TEG}$ and $\ddot{v}_{TEG}$ are the first and second time derivatives of TEG voltage respectively. By solving equation (21), the value of the duty-cycle for MPPT of TEG source can be updated in the proposed Lyapunov-based nonlinear controller. In Appendix II, a mathematical proof for the asymptotic stability of proposed controller is presented. Hence, the controller in equation (16) can stabilize the boost DC-DC converter satisfactorily despite temperature changes in a wide range. In the next section, the simulation and experimental responses of developed controller are studied.

4- Simulation and experimental results

To evaluate the performance and effectiveness of proposed approach in the wide range of changes, a TEG simulator is employed in both simulation and experimental tests. The simplified structure of simulator and boost DC-DC converter are shown in Fig.8. Considering the equivalent circuit model of TEG devices in Fig.1, a voltage source with a series resistor can be employed as a TEG simulator which is shown in Figure 7-a. It should be noted that $R_{TEG} = 1.5ohm$ and $V_{OC} = 10V$ represent the internal resistance and open-circuit voltage of TEG in the nominal temperature. Since the values of R_{TEG} and

V_{TEG} are changed with temperature, three semiconductor switches (S_1, S_2 and S_3) are employed in the simulator circuit to enable step changes in TEG parameters. By using the S_1 in Fig.8-a, it is seen that the TEG resistance can be switched between *1.35ohm* and *2.3ohm*. Also, switches S_2 and S_3 can be used for step changes of the open-circuit voltage between *10V* and *14V*. Steady-state and dynamic responses of the designed controller are studied for step changes of TEG model parameters. It should be noted that the proposed controller is simulated using Matlab/Simulink software.

Moreover, the TMS320F28335 digital signal processor (DSP) which has been released by Texas instruments is employed for the practical implementation of proposed controller. The block diagram of experimental setup is shown in Fig.8-b. By using the isolated Hall-Effect current and voltage sensors, the feedback signals are sent to the DSP board through the internal Analogue-to-Digital converters. Then, the real-time value of TEG power is calculated as the main feedback signal of controller in the DSP chip. Considering the developed controller in equation (21), the converter duty cycle is calculated in the DSP and transmitted to the gate driver circuit through the PWM unit. Despite the temperature and parameters changes, the controller reference value is always zero and any additional loops are not required for the calculation of reference signal. The FAN8811 gate-drive IC from the ON Semiconductor is employed to provide current amplification as well as optic isolation between the DSP board and power converter. Also, the IRF1104PBF and IRPP460 are used as a power MOSFET and diode

respectively, in both the TEG simulator and main converter. The details of load and inductor are shown in Fig.8-b. Finally, it should be noted that the switching and sampling frequencies of the designed system are equal to 20kHz and 200kHz respectively.

Test 1- Start-up and shut-down responses of the developed controller

In this test, the start-up and shut-down responses of proposed controller are studied for nominal conditions. According to the TEG simulator in Fig.8-a, the switches S_1 and S_2:are assumed to be OFF and S_3:is ON. Hence, the open-circuit voltage and internal resistance of TEG are *14V* and *1.5ohm* respectively. So based on equations (5) and (6), the MPP of TEG source will be equal to $V_{TEG}=7V$ and $I_{TEG}=4.67A$. Simulation and experimental responses of the proposed control approach in start-up conditions are shown in Fig.9 and Fig.10 respectively. It is observed that while the MPPT controller is not enabled, the TEG source current is zero and $V_{TEG}=14V$. On the other hand, once the controller starts, the operating point of closed-loop system is settled at the mentioned MPP. It is seen that the proposed controller can track the MPP of TEG source stably with zero steady-state error. Finally, it enjoys an acceptable dynamic response and any overshoot isn't seen during the converter start-up.

Also, the shut-down response of designed controller is illustrated in Fig.11 (simulation) and Fig.12 (experimental). At first, it is assumed that the TEG source operates at the

MPP. Then, the controller is stopped by forcing the duty cycle to zero. It is seen that the converter stops smoothly with acceptable dynamic and steady-state responses.

Test 2- Internal resistance changes

In Fig.8-a, the S_1 is switched ON and OFF periodically to emulate the internal resistance changes of TEG source. In this test, the simulation and experimental responses of developed controller are illustrated in Fig.13 and Fig.14 respectively. It is assumed that the open-circuit voltage of TEG source is 14V. Since the value of resistance is switched between *1.5ohm* and *2.3ohm*, as a result, the TEG current at MPP will change between *4.67A* and *3A* respectively. Also, the output power of TEG source is equal to *32.69W* (for *1.5ohm*) and *21.3W* (for *2.3ohm*). According to the simulation results and despite 50% changes in the internal resistance, the operating point of TEG is placed at MPP and the output voltage of TEG source (V_{TEG}) is stabilized on the reference value ($\frac{V_{TEG}}{2} = 7V$).

Test 3- Input voltage changes

Simulation and experimental responses of the designed closed-loop system to the step changes of TEG voltage are illustrated in Fig.15 and Fig.16 respectively. In this test, the internal resistance of TEG source and battery voltage are *1.5ohm* and *25V* respectively. The open-circuit voltage of TEG source is stepped between *10V* and *14V* by

complementary switching of S_2 and S_3 in Fig.8-a. In this condition, the current of TEG source at the MPP is equal to *3.33A* and *4.67A* respectively. Also, the output power of generator is *16.65W* and *32.67W*. Despite 40% changes in the open-circuit voltage, it is seen that the proposed controller is stable and robust against parameter changes with zero steady-state error. It should be noted that the response settling time for the step changes of TEG open-circuit voltage is about *0.04 sec.*

Also in this test, the response of proposed controller is compared with the two-loop controllers. According to Fig.6, a P&O approach is employed for the calculation of TEG reference voltage at MPP and a PI controller is used in the inner loop of two-loop MPP controller. It is assumed that the voltage steps of P&O method are *0.1V* and the proportional and integral gains of PI controller are *0.5* and *3* respectively. Considering Test-3, the response of mentioned two-loop controller for step changes of TEG open-circuit voltage is illustrated in Fig.15-b. It is seen that the response setting time is *0.09 sec.*

According to the simulation results in Fig.15, it can be concluded that:

1- The dynamic response of proposed controller is faster than the two-loop controller.
2- The steady-state fluctuation of P&O approach can be removed using the developed nonlinear controller.

Conclusion: Considering the nonlinear characteristic of DC-DC boost converter, the Lyapunov-based nonlinear controller is developed for MPPT of TEG sources. A systematic model-based approach is proposed for controller design which is based on the state-space averaged model of converter. Since the time-derivative of TEG power is used as the feedback signal, the reference value of controller is always zero and hence, an additional loop isn't needed for reference calculation. As a result, the proposed single-loop controller enjoys a fast dynamic response for the MPPT of TEG sources. Moreover, no perturbations will be needed during the steady-state operation of converter which can improve the power efficiency of system. The stability of proposed controller is proved in the whole operational range of converter by using the Lyapunov and Barbalat stability criteria. Based on the simulation and experimental results, it is demonstrated that the proposed control approach is robust against temperature, and model parameters changes. Also, the steady-state error of closed-loop system is zero in different operational conditions. It should be noted that for the large TEG-based power plants, some local MPPs might be seen due to considerable changes in the module's temperature. In such an application, the power derivative approach which has been developed in this paper should be revised in future research to distinguish the global MPP.

References

1. Ibrahim, M., Rezk, H., Al-Dahifallah, M., et al. "Hybrid Photovoltaic-Thermoelectric Generator Powered Synchronous Reluctance Motor for Pumping Applications," *IEEE Access* 7(1): 146979-146988. (2019).

2. Panwar, N., and Himanshu, K. " Waste heat recovery from improved cookstove through thermoelectric generator," *International Journal of Ambient Energy* 1(1): 321-329. (2019).

3. Anandasabesan, A., Mahamani, S., Soundararajan, H., et al. "Work-in-Progress: Smart Automatic Regeneration of Electricity using Thermoelectric Generator Technology," *2021 4th International Conference on Computing and Communications Technologies (ICCCT)*, pp. 484-488, (2021).

4. Yahya, K, and Alomari, O. "A new maximum power point tracking algorithm based on power differentials method for thermoelectric generators." *Int J Energy Res*. ; 45: 7476– 7486, (2021).

5. Montecucco, A. and Knox, A. "MPP Tracking Converter Based on the Open-Circuit Voltage Method for Thermoelectric Generators," *IEEE Transactions on Power Electronics* 30(2): 828-839. (2015).

6. Ranjana, A. "Thermodynamic investigations with MPP tracking (MPPT) of hybrid thermoelectric generator-heat pump" model, International Journal of Ambient Energy" 10.1080/01430750.2020.1739140, (2020)

7. Hernández-Díez, J., Méndez-Barrios, C., Niculescu, S., et al. "A Current Sensorless Delay–Based Control Scheme for MPPT–Boost Converters in Photovoltaic Systems," in *IEEE Access*, vol. 8, pp. 174449-174462, (2020).

8. Dadkhah, J., and Niroomand, M. "Optimization Methods of MPPT Parameters for PV Systems: Review, Classification, and Comparison," *Journal of Modern Power Systems and Clean Energy* 9(2): 225-236. (2021).

9. Selmi, T., Abdul-Niby, M., Devis, L., et al. "P&O MPPT implementation using MATLAB/Simulink," *Ninth International Conference on Ecological Vehicles and Renewable Energies (EVER)* 1-4. (2014).

10. Aslam, H., and Tariq, A. "Transient analysis and selection of perturbation parameters for PV-MPPT implementation," International Journal of Ambient Energy, 41 (10): 1176-1182. (2020).

11. Aldhaifallah, M., Saif, A., Baroudi, U., et al. "Fractional Incremental Resistance Based MPPT for Thermoelectric Generation systems," *18th International Multi-Conference on Systems, Signals & Devices (SSD)* 902-907. (2021).

12. Bhattacharyya, S., Kumar, P., Samanta, S., et al. "Steady Output and Fast Tracking MPPT (SOFT-MPPT) for P&O and InC Algorithms," *IEEE Transactions on Sustainable Energy*. 12(1): 293-302. (2021).

13. Bertin, C., Wira,P., Kamta, M., et al." Real-Time Experimental Assessment of Hill Climbing MPPT Algorithm Enhanced by Estimating a Duty Cycle for PV System," *International Journal of Renewable Energy Research, IJRER*, 9(3): 1180-1189. (2019).

14. Karthika, S., Asok, M., Mohan, M., et al. "An Enhanced P and O Algorithm for MPP Tracking," *International Conference on Futuristic Technologies in Control Systems & Renewable Energy (ICFCR)* 1(1): 1-6, (2020).

15. Jiandong, D., Ma, X. and Tuo, S. "A Variable Step Size P&O MPPT Algorithm for Three-Phase Grid-Connected PV Systems," *China International Conference on Electricity Distribution (CICED)* 1997-2001, (2018).

16. Divyasharon, R., Narmatha, R., and Devaraj, D. "Artificial Neural Network based MPPT with CUK Converter Topology for PV Systems Under Varying Climatic" *Optimization and Signal Processing (INCOS)* 1-6, (2019).

17. Hariz, Z., Aissaoui, H. and Diany, M. "A novel optimiser of MPPT by using PSO-AG and PID controller" *International Journal of Ambient Energy* 1(1): 1-8, (2021).

18. Hoang, T., Nguyen, X., Le, A., et al. "Power generation characteristics of a thermoelectric modules-based power generator assisted by fishbone-shaped fins: Part II – Effects of cooling water parameters," *Energy Sources, Part A: Recovery, Utilization, and Environmental Effects,* 43(3): 381-393, (2019).

19. Mirza, A., Mansoor, M., Zerbakht, K., et al. "High-efficiency hybrid PV-TEG system with intelligent control to harvest maximum energy under various non-static operating conditions", *Journal of Cleaner Production*, Volume 320, (2021).

20. Bollipo, R., Mikkili S., and Bonthagorla, P. "Hybrid, optimal, intelligent and classical PV MPPT techniques: A review," in *CSEE Journal of Power and Energy Systems*, vol. 7, no. 1, pp. 9-33, Jan, (2021).

21. Zhang, X., Yang, B., Yu, T., et al. "Dynamic Surrogate Model Based Optimization for MPPT of Centralized Thermoelectric Generation Systems Under Heterogeneous Temperature Difference," *IEEE Transactions on Energy Conversion* 35(2): 966-976, (2020).

22. Sudwilai, P. "A Design and Development of P I Controlled Based MPPT for Photovoltaic Systems," *2018 21st International Conference on Electrical Machines and Systems (ICEMS)*, pp. 992-995, (2018).

23. Lawan, A., Magaji, N., and Musa, H. "A STATCOM controller for small signal stability using polynomial algorithms in a horizontal axis wind farm power system," *IEEE Energy tech* 1(1): 1-5, (2013).

24. Kabalci, E., Gokkus, G., and Gorgun, A. "Design and implementation of a PI-MPPT based Buck-Boost converter," *2015 7th International Conference on Electronics, Computers and Artificial Intelligence (ECAI)*, Bucharest, Romania, , pp. SG-23-SG-28, (2015).

25. Kumar. M., Satya, S., and Vulasala, G. "Advanced sliding mode control for solar PV array with fast voltage tracking for MPP algorithm," *International Journal of Ambient Energy*, 41(10): 1192-1200, (2018).

26. Pradhan, R. and Subudhi, B. "Double Integral Sliding Mode MPPT Control of a Photovoltaic System," *IEEE Transactions on Control Systems Technology* 24(1): 285-292, (2016).

27. Kamal, T., Karabacak, M., Hassan, S., et al. "A Robust Online Adaptive B-Spline MPPT Control of Three-Phase Grid-Coupled Photovoltaic Systems Under Real Partial Shading Condition," *IEEE Transactions on Energy Conversion* 34(1): 202-210, (2019).

28. Veisi, A., and Delavari, H. "Adaptive Fractional order Control of Photovoltaic Power Generation System with Disturbance Observer," *7th International Conference on Control, Instrumentation and Automation (ICCIA*) 1-5, (2021).

29. Wang, N., Zhang, J., Ni, H., et al. "Improved MPPT System Based on FTSMC for Thermoelectric Generator Array Under Dynamic Temperature and Impedance," in *IEEE Transactions on Industrial Electronics*, vol. 69, no. 10, pp. 10715-10723, Oct., (2022).

30. Bond, M. and Park, J. "Current-Sensorless Power Estimation and MPPT Implementation for Thermoelectric Generators," in IEEE Transactions on Industrial Electronics, vol. 62, no. 9, pp. 5539-5548, Sept., (2015).

31. Abdelsalam, A., Massoud, A., Ahmed, S., et al. "High-Performance Adaptive Perturb and Observe MPPT Technique for Photovoltaic-Based Microgrids," in *IEEE Transactions on Power Electronics*, vol. 26, no. 4, pp. 1010-1021, April 2011, (2011).

Fig.1: Equivalent electric model of TEG

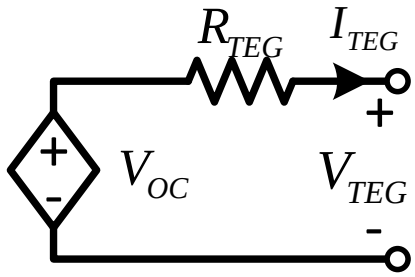

Fig.2: Current-voltage and power-voltage characteristics of a typical TEG for different temperatures (M. Bond and J. Park, 2015)

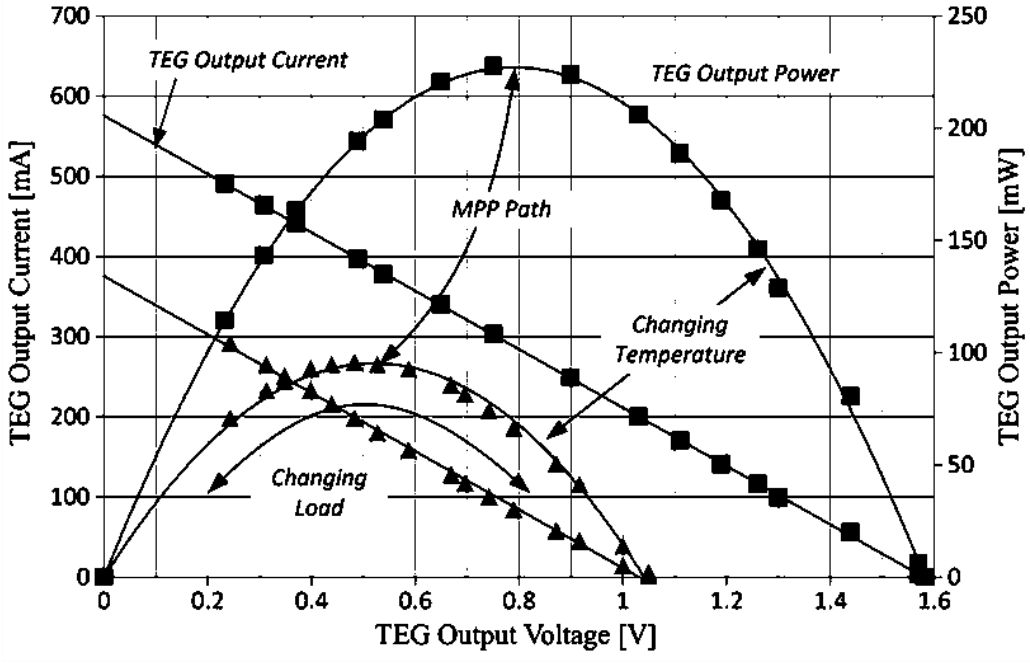

Fig.3: The output power of TEG depends on the external load

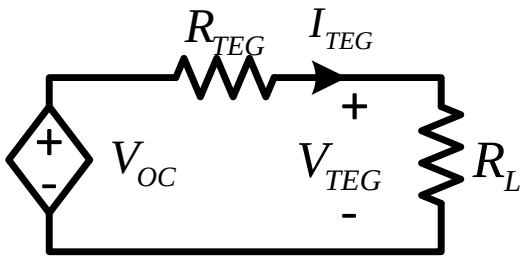

Fig.4: Application of the TEG as an input power source of boost DC-DC converter

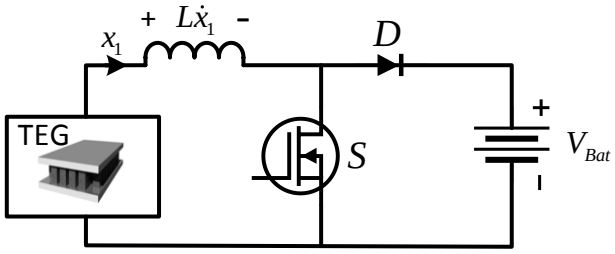

Fig.5: Equivalent circuits of the boost DC-DC converter in continuous conduction mode

(a) The power switch (S) is ON.

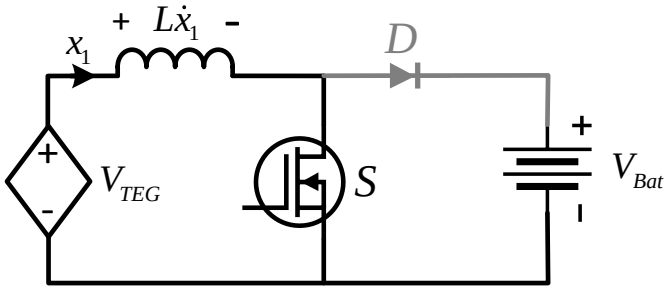

(a) The power switch (S) is OFF.

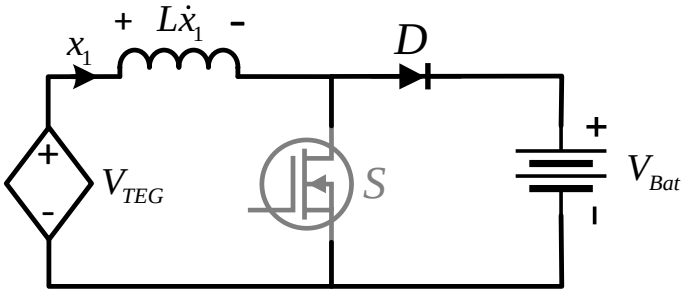

Fig.6: Two-loop controller forMPPT of TEG sources

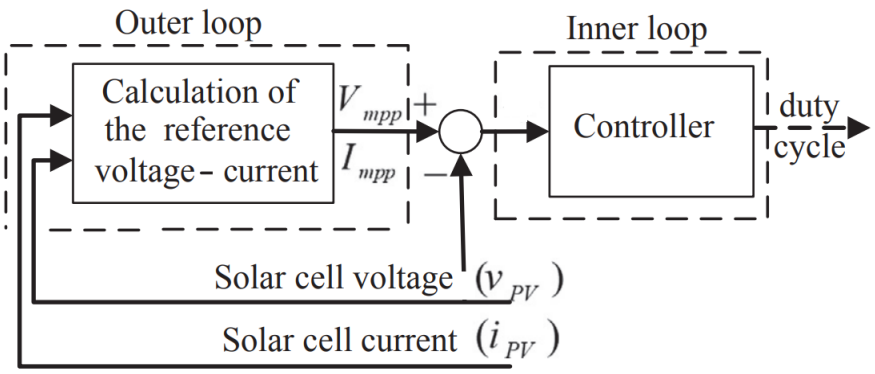

Fig.7: The block diagram of proposed Lyapunov-based nonlinear controller

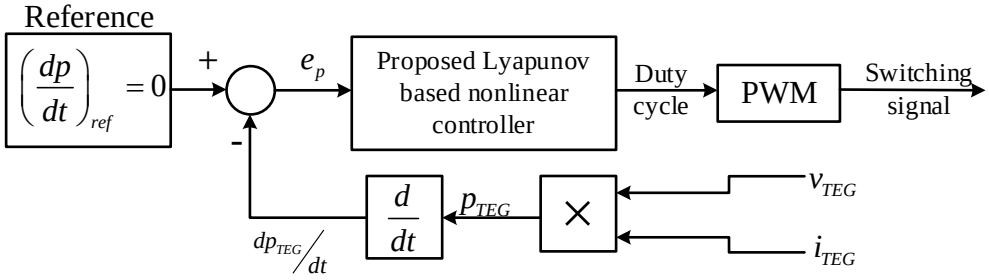

Fig.8: Detail of the implemented controller

(a) The power circuit of TEG simulator and main converter

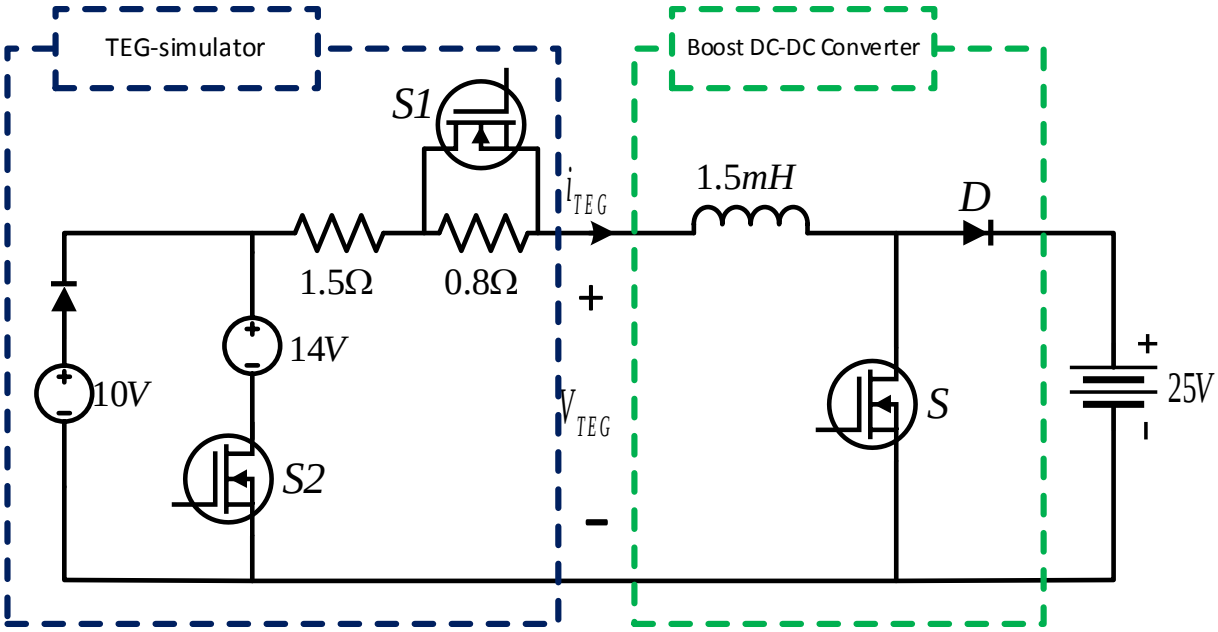

(a) Block diagram of the experimental setup

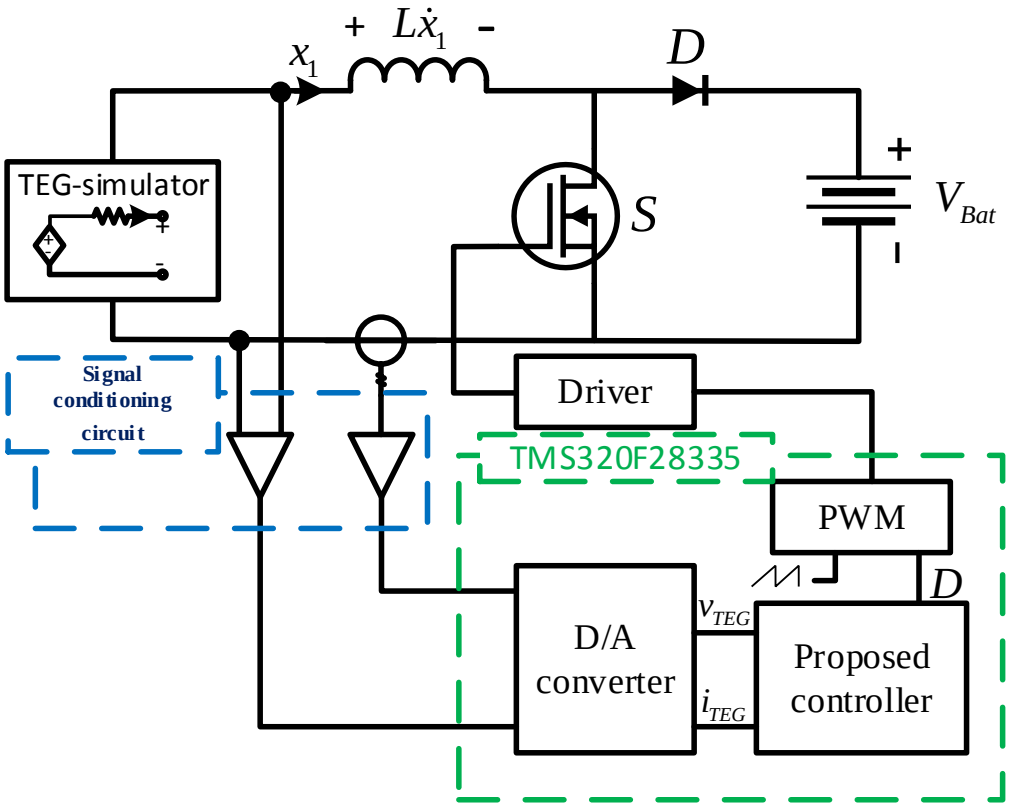

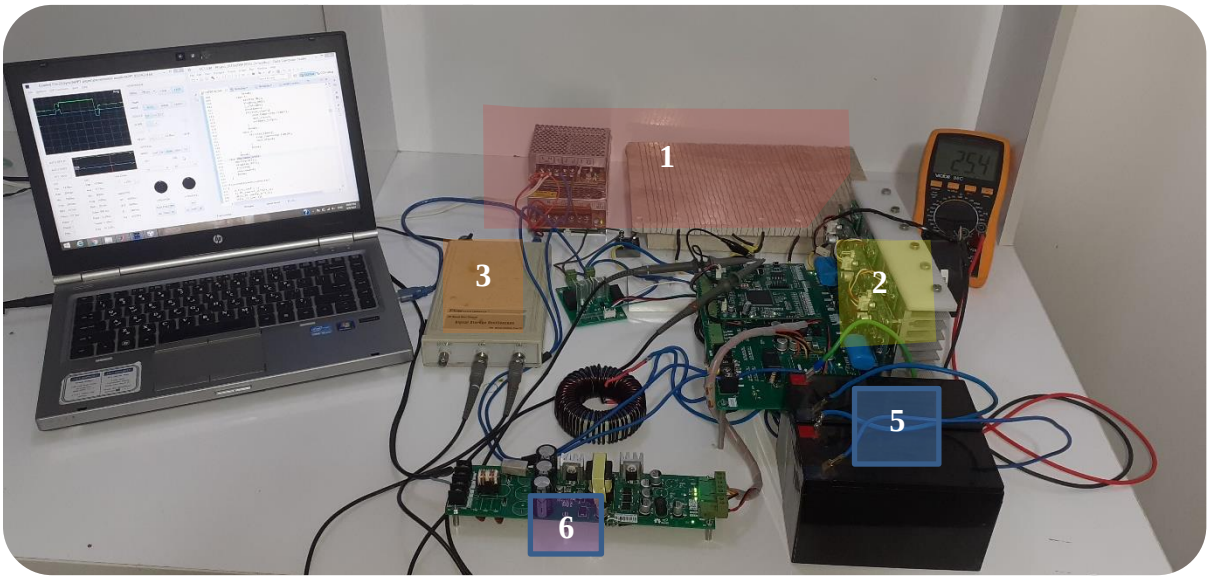

(b) Experimental setup

Fig.9: Dynamic response of the proposed controller during start-up (simulation)

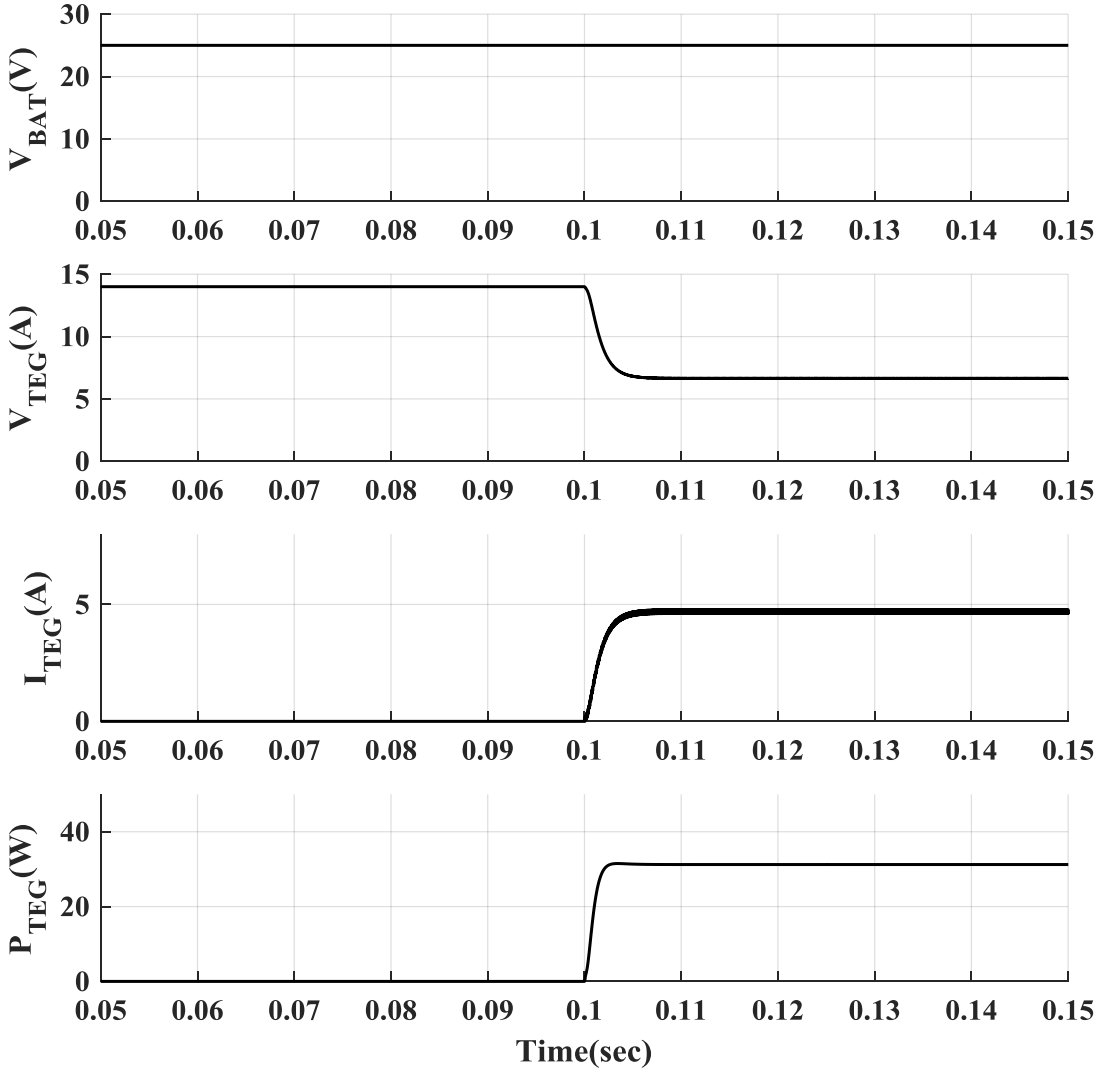

Fig.10: Response of the proposed controller during the converter start-up (experimental)

a) Output voltage (V_{TEG}, blue waveform, *5V/Div*.) and current (I_{TEG}, Green waveform, *3.7A/Div.)* of TEG source. Time-division is *5ms*.

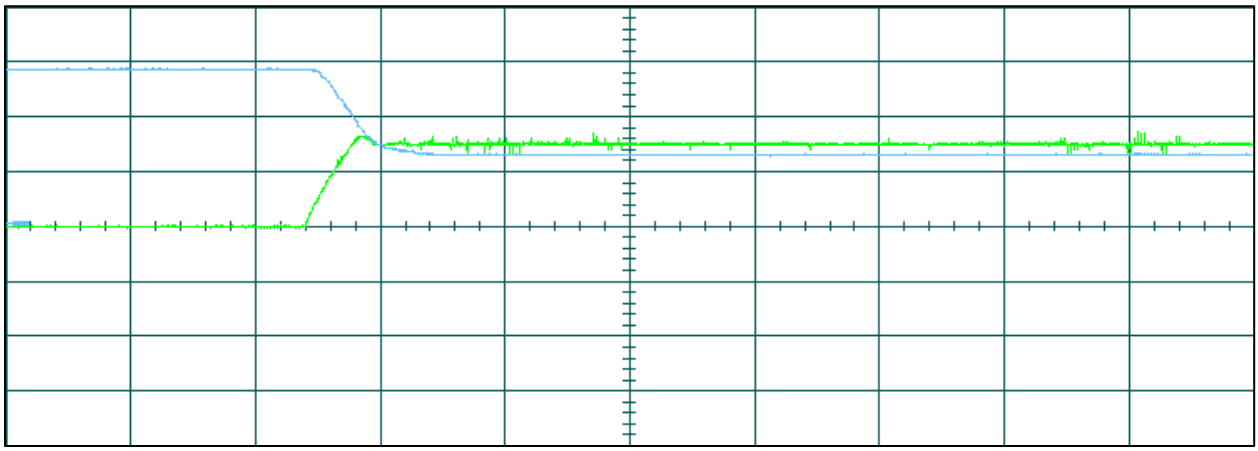

b) Output voltage (V_{TEG}, blue waveform, *10V/Div*.) of TEG source and load voltage (V_{BAT}, Green waveform, *10V/Div*.). Time-division is *5ms*.

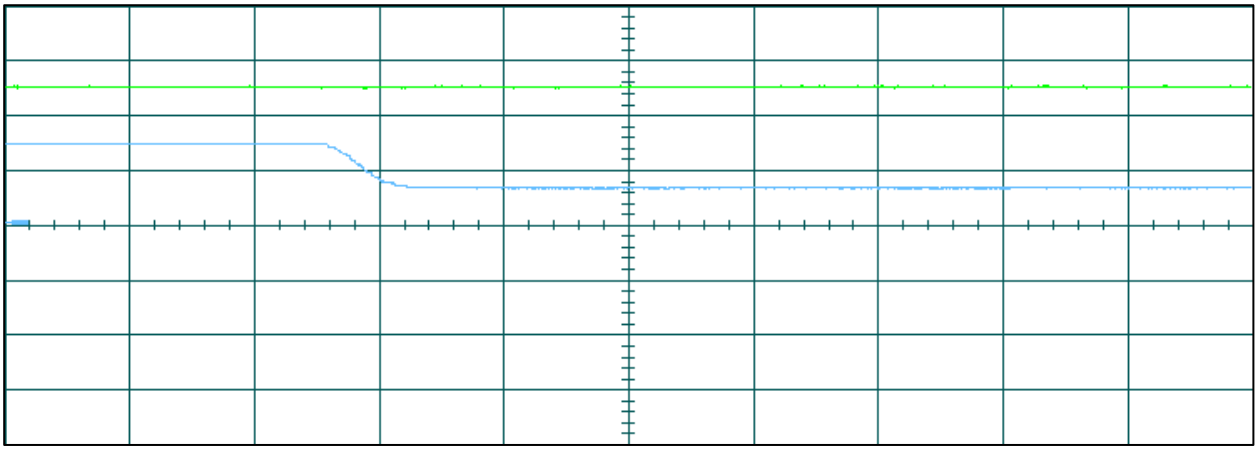

c) Output power (P_{TEG}, blue waveform, *25W/Div*.) and current (I_{TEG}, Green waveform, *7.2A/Div*.) of the TEG source. Time division is *5ms*.

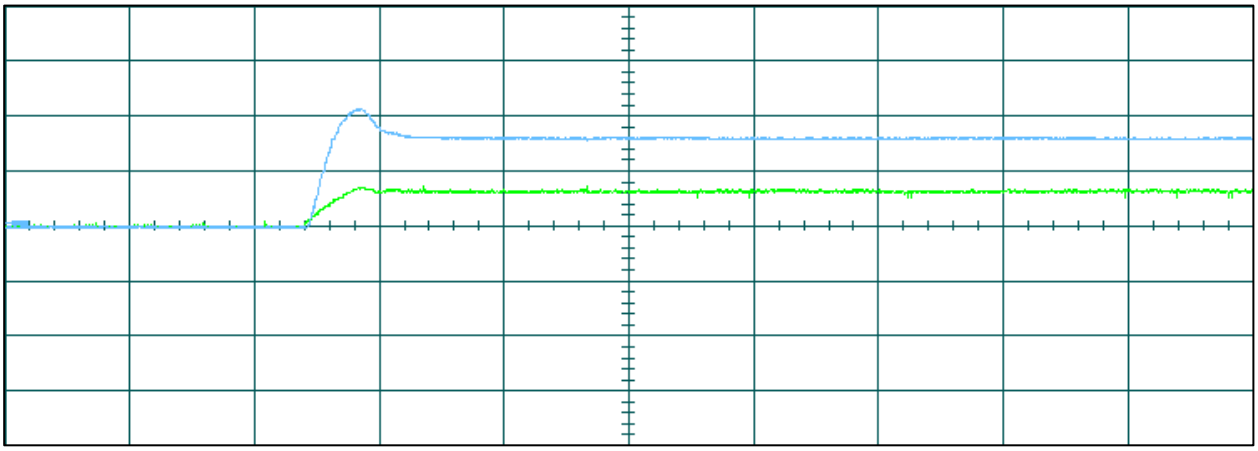

Fig.11: Shut-down response of the controller (simulation)

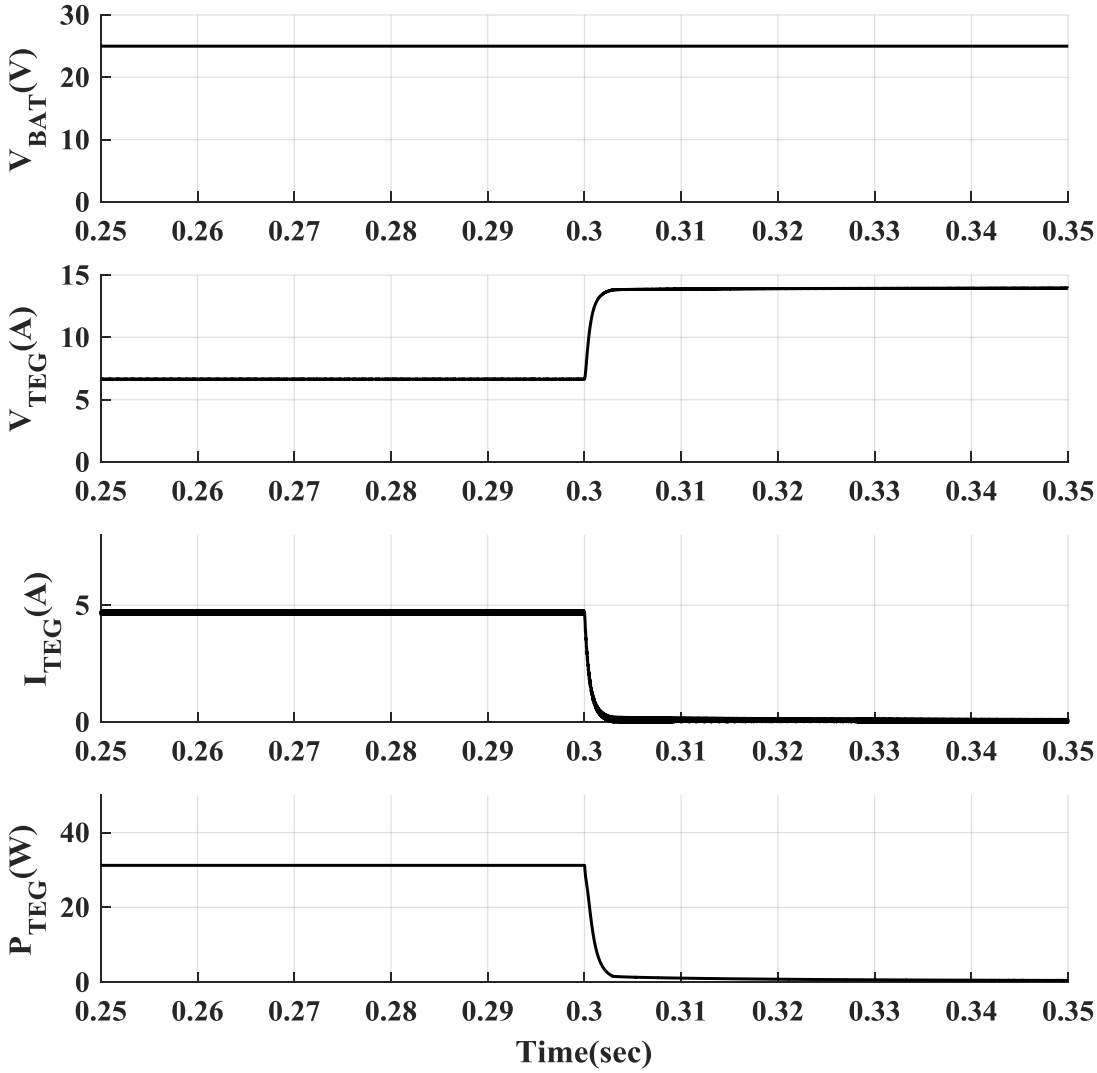

Fig.12: Experimental shut-down response of the converter. Output voltage (V_{TEG}, blue waveform, *5V/Div*.) and current (I_{TEG}, Green waveform, *3.7A/Div*.) of the TEG source are shown. Time division is *5ms*.

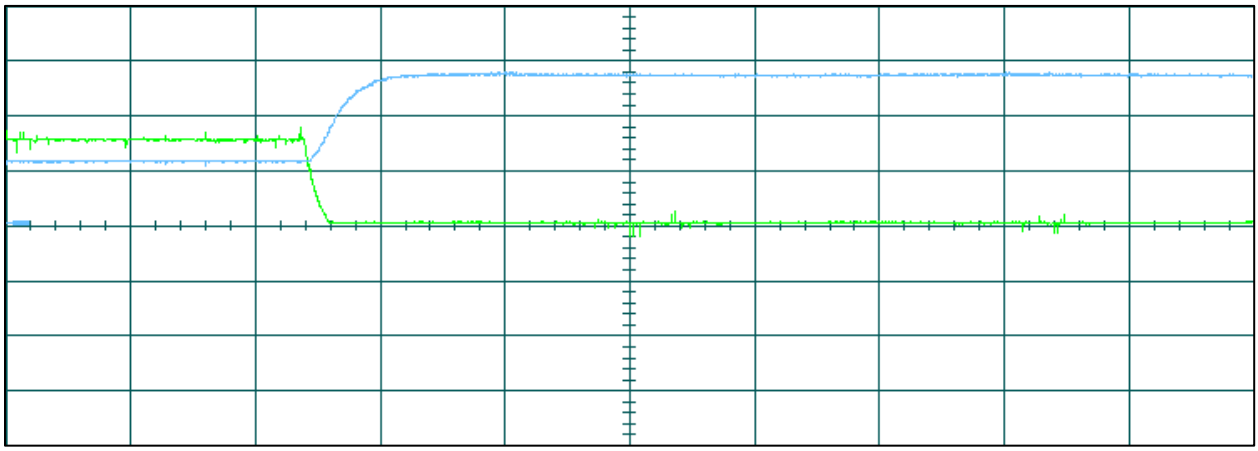

Fig.13: Simulation of the controller during periodic changes of TEG internal resistance

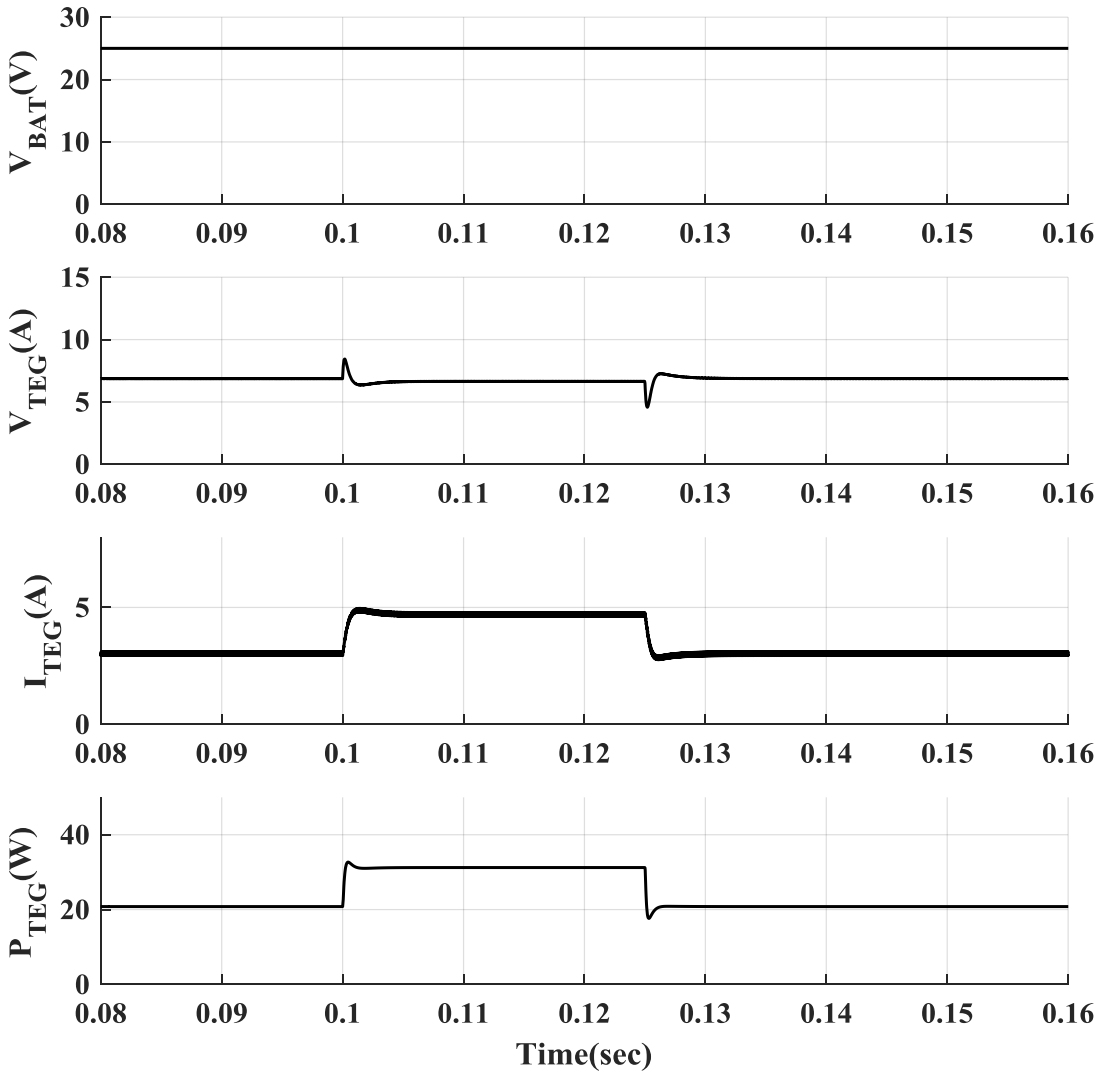

Fig.14: Experimental response of controller during the step changes of TEG internal resistance

(a) Output voltage (V_{TEG}, blue waveform, *2.5V/Div*.) and current (I_{TEG}, green waveform, *3.75A/Div*.) of TEG source. Time division is *5ms*.

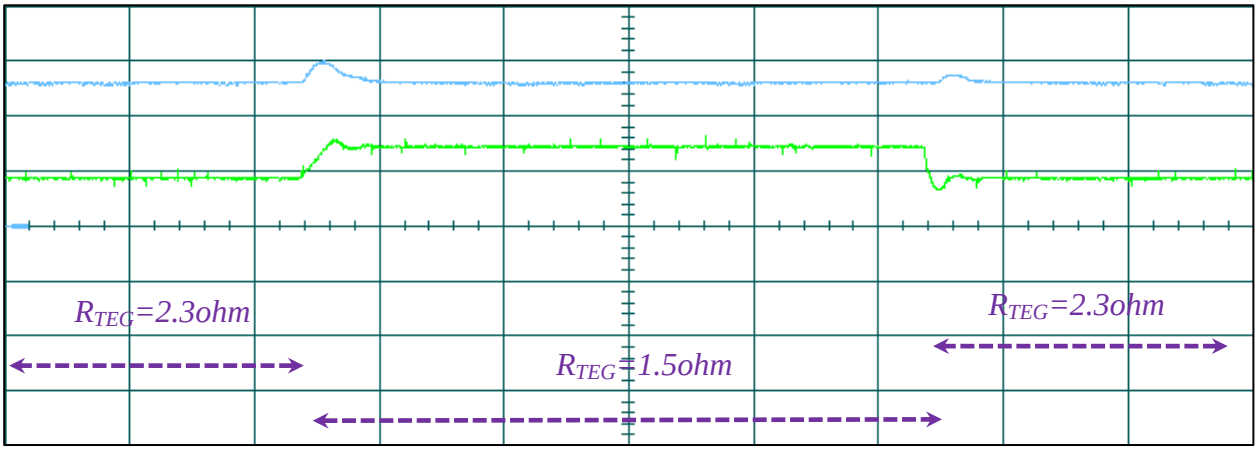

(b) Output power (P_{TEG}, blue waveform, *10W/Div*.) and current (I_{TEG}, green waveform, *3.75A/Div*.) of TEG source. Time-division is *5ms*.

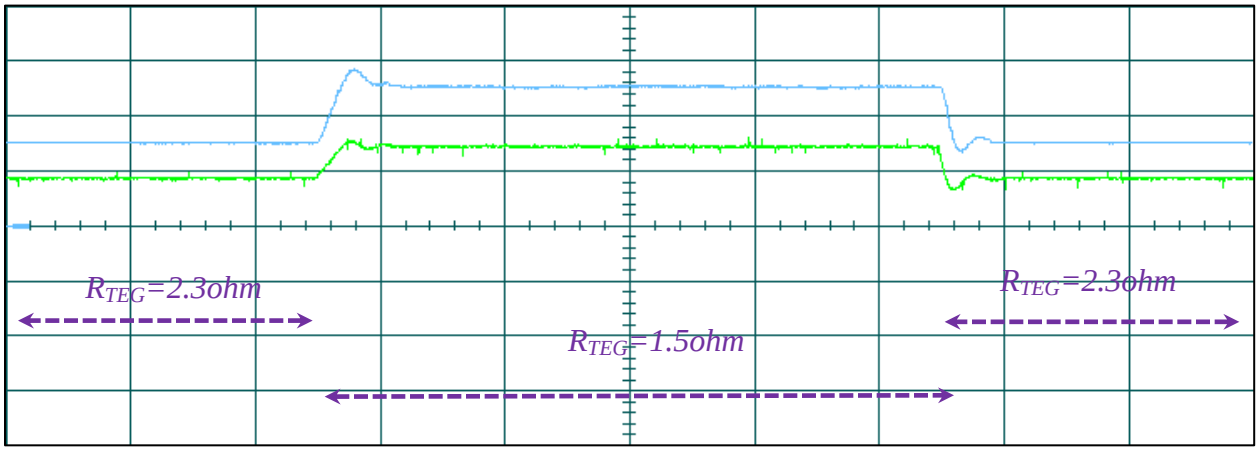

Fig.15: Simulation responses of the developed and traditional controllers to step changes of TEG voltage

(a) Response of the developed controller

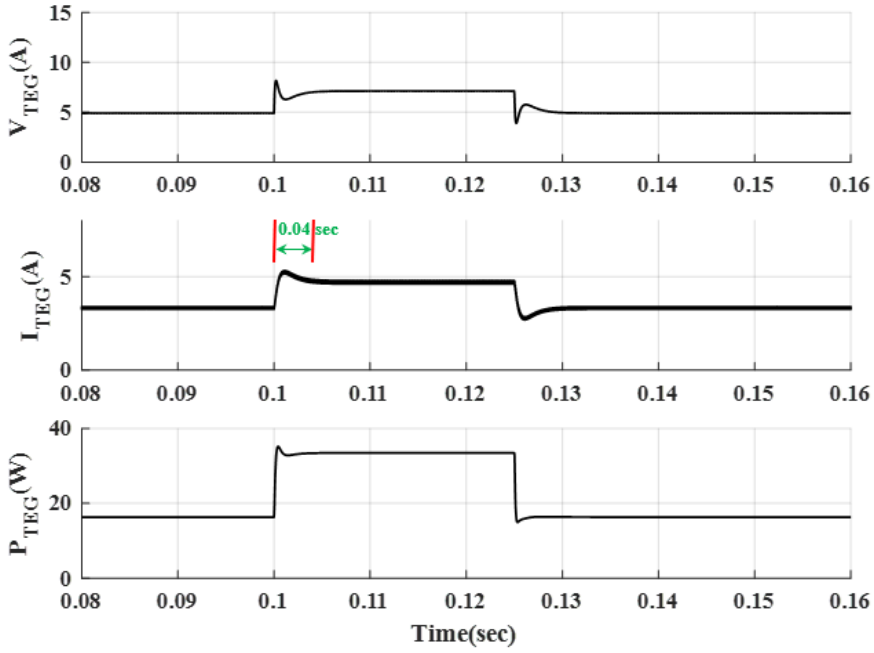

(b) Response of the two-loop P&O-based MPPT controller

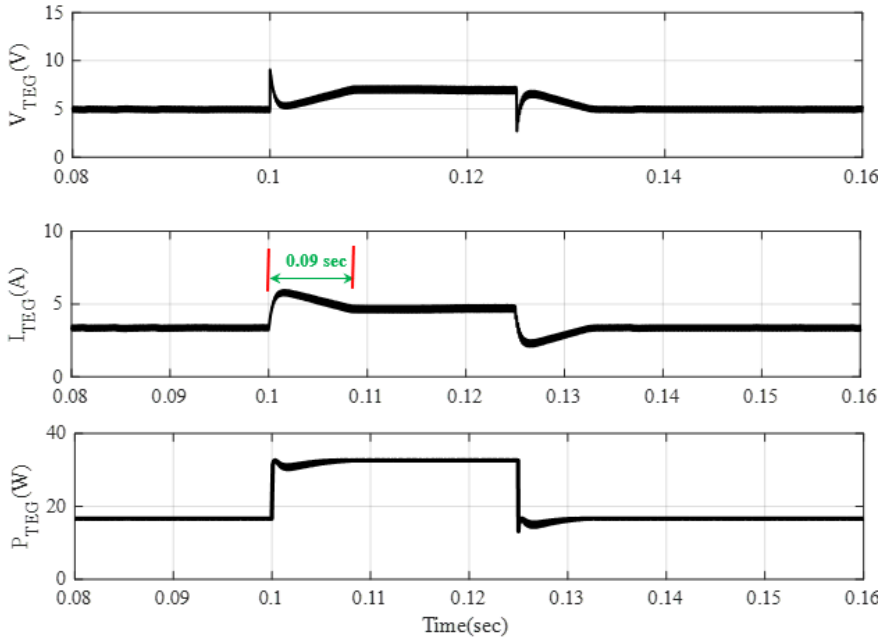

Fig.16: Experimental response of controller to step changes of TEG voltage

(a) Output voltage (V_{TEG}, blue waveform, *2.5V/Div*.) and current (I_{TEG}, Green waveform, *3.75A/Div*.) of TEG source. Time division is *5ms*.

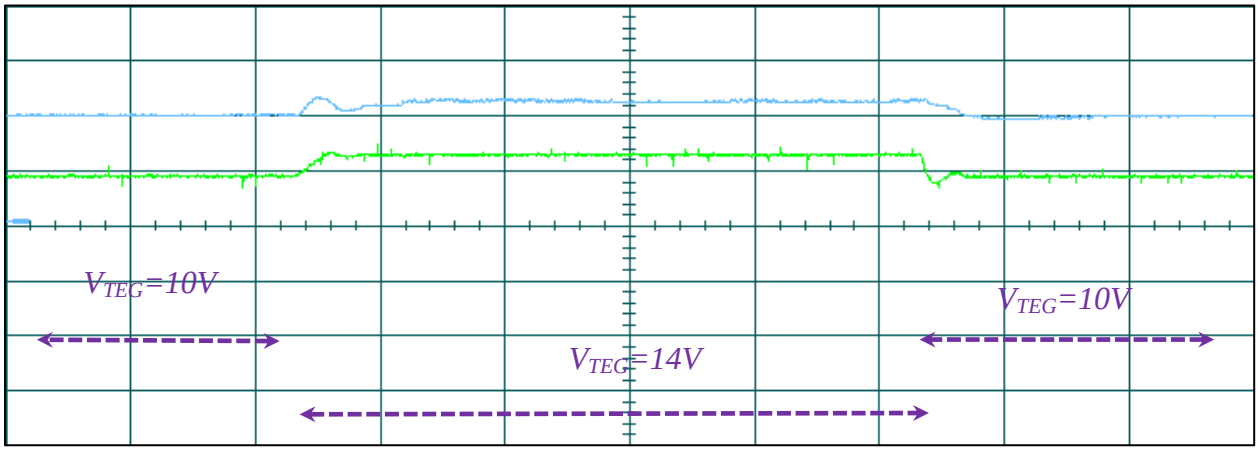

(b) Output power (P_{TEG}, blue waveform, *10W/Div*.) and current (I_{TEG}, green waveform, *3.75A/Div*.) of the TEG source. Time division is *5ms*.

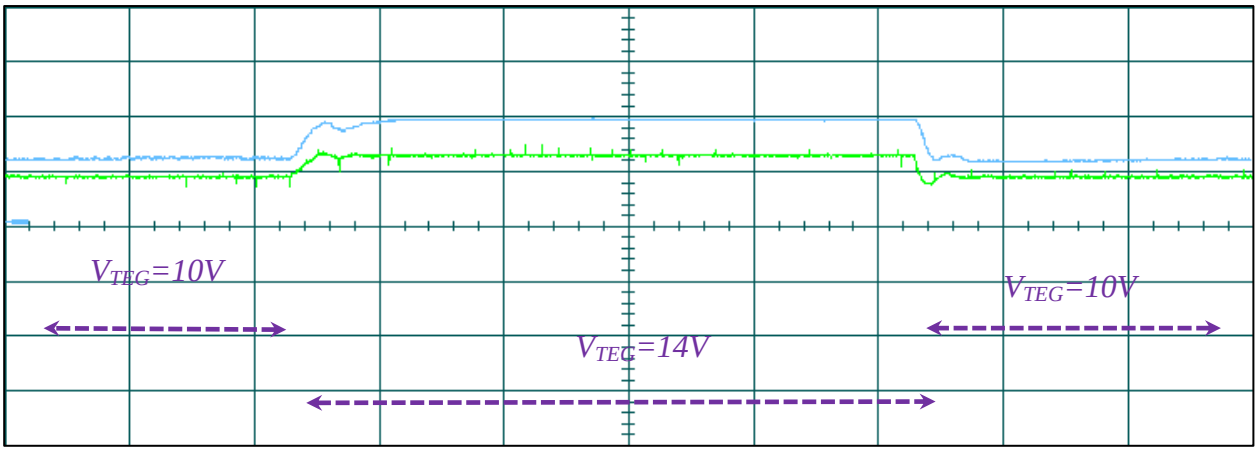

Fig.17: Switching signal of DC-DC converters

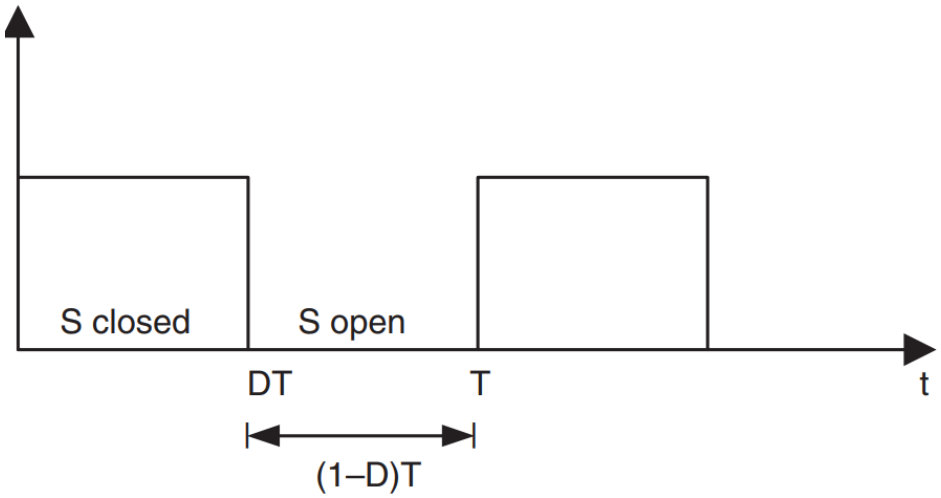

Appendix I: Averaged state-space modelling of DC-DC converters

In this section, the details of averaged state-space modelling for DC-DC converters are explained. As the main switch of converter will be either ON or OFF, the operation of converter can be modelled using two different sub-circuits in continuous conduction mode. Assuming x_g as a switching signal ($x_g = 0$ for the off-state and $x_g = 1$ for the on-state) in Fig.17 and the state-space models for each subcircuit can be written as:

Sub-circuit(1): where $x_g = 1$ and $0 < t < DT$ $\quad \dot{X} = A_1 X + B_1$ (22)

Sub-circuit(0): where $x_g = 0$ and $DT < t < T$ $\quad \dot{X} = A_0 X + B_0$ (23)

where T is the switching period and D is the duty cycle.

These two models can be combined to form the switched state-space model as follows:

$$\dot{X} = A_s X + B_s \qquad (24)$$

where:

$$A_s = x_g A_1 + (1 - x_g) A_0 \qquad (25)$$

$$B_s = x_g B_1 + (1 - x_g) B_0 \qquad (26)$$

To extract the averaged model, the generic solutions of (22) and (23) are presented below.

$$X_1(t) = e^{A_1 t} X_1(0) + \int_0^t e^{A_1 (t-\tau)} B_1 d\tau \qquad (27)$$

$$X_0(t) = e^{A_0(t-t_1)}X_0(t_1) + \int_{t_1}^{T} e^{A_0(t-\tau)}B_0 d\tau \qquad (28)$$

Defining $M_i(t) \triangleq \int_0^t e^{A_i(t-\tau)}d\tau = A_i^{-1}(e^{A_i t} - I)$, the equations (27) and (28) can be simplified.

$$X_1(t) = e^{A_1 t}X_1(0) + B_1 M_1(t) \qquad t \in [0, t_1] \qquad (29)$$

$$X_2(t) = e^{A_2(t-\tau)}X_2(0) + B_0 M_0(t) \qquad t \in [t_1, T] \qquad (30)$$

Since the equations are continuous and $X_1(t_1) = X_0(t_1)$:

$$X_0(T) = e^{A_0(1-D)T}e^{A_1 DT}X_1(0) + e^{A_0(1-D)T}[M_1(DT)B_1 + M_0((1-D)T)B_0] \qquad (31)$$

Moreover:

$$e^{AT} = I + AT + A^2\frac{T^2}{2} + A^3\frac{T^3}{2} + ... \qquad (32)$$

In DC-DC converters, the time constant of the closed-loop system is far less than the switching frequency. So, it can be assumed that $\lambda_{\max}T << 1$, where $\lambda_{\max}$ is the maximum of the absolute values of all eigenvalues of A. So, the equation (32) can be approximated as:

$$e^{AT} \cong I + AT \qquad (29)$$

Considering (29), the equation (31) can be simplified as follows:

$$X_0(T) = [I + DTA_1 + (1-D)TA_0]X_1(0) + [DTB_1 + (1-D)TB_0] \qquad (30)$$

or:

$$\frac{X_0(T)-X_1(T)}{T}=[DA_1+(1-D)A_0]X_1(0)+[DB_1+(1-D)B_0] \qquad (31)$$

Since $\dot{X}=\frac{X_0(T)-X_1(T)}{T}$, the averaged state-space model of converter can be obtained. In this equation, the parameter $0\le D\le 1$ is the duty cycle of switching signal.

$$\dot{X}=AX+B \qquad (32)$$

$$A=DA_1+(1-D)A_0 \qquad (33)$$

$$B=DB_1+(1-D)B_0 \qquad (34)$$

Appendix II: Stability analysis of the proposed nonlinear controller

The control effort of the proposed Lyapunov based nonlinear controller is presented in the equation (21). The asymptotic stability of controller can be proved using the Brbalat Lemma. If the selected scalar Lyapunov function $V=V(t,z)$ satisfies the following conditions (where t is time and z is the error variable), the asymptotic stability of closed-loop system will be proved.

- $V(t,z)$ must be a lower bounded function. Considering the selected Lyapunov function as $V(t,z)=\frac{1}{2}z^2$, its minimum value is zero and hence, it is lower bounded.
- The time derivative of Lyapunov function $\dot{V}(t,z)$, must be a negative semi-definite function. This condition has been proved in the paper as well.

Considering the equation (20), it can be seen that $\dot{V}(t,z) = -cz^2$. As a result, $\dot{V}(t,z) \leq 0$.

- $\dot{V}(t,z)$ must be a uniformly continuous function. To verify it, the second time derivative of Lyapunov function will be:

$$\ddot{V} = -2cz\dot{z} \qquad (35)$$

Now by placing $\dot{z}$ from equation (14) in (35):

$$\ddot{V} = -2cz\left(\frac{2}{L}v_{TEG}\dot{v}_{TEG} - \frac{\dot{D}}{L}v_{TEG}V_{Bat} + \frac{1-D}{L}\dot{v}_{TEG}V_{Bat} - \ddot{v}_{TEG}x_1 - \frac{\dot{v}_{PV}}{L}(v_{TEG} - (1-D)V_{Bat})\right) \quad (36)$$

Since the error variable and other parameters of the model are finite, it can be concluded that $\ddot{V}$ has a finite value and is bounded. As a result, $\dot{V}(t,z)$ will be uniformly continuous.

According to the Barbalat lemma, as all the conditions are satisfied, then it can be concluded that $\dot{V}(t,z) \longrightarrow 0$, as $t \longrightarrow \infty$. Considering $\dot{V}(t,z) = -cz^2$, it can be concluded that $\dot{V}(t,z) \longrightarrow 0$ means that the error variable tends toward zero $z \longrightarrow 0$ as $t \longrightarrow \infty$.Hence, the asymptotic stability of proposed nonlinear controller is proved.

Biographies

Sarah Kowsari Mogadam completed her B.Sc study in communication engineering at Islamic Azad University - Urmia Branch in 2005 and her M.Sc study in power engineering at Islamic Azad University – Ardebil Branch. During her M.Sc studies, she designed and implemented a novel grid-connected photovoltaic system for the Engineering faculty in 2017. Also, she introduced a new index for the identification of the maximum consumption rate for the Ardabil electricity distribution network. she is currently a PhD student at the Islamic Azad University - Ardabil Branch. The main objective of her PhD thesis is to design, implement and develop a nonlinear controller for thermal energy recovery using Thermoelectric Generators (TEG) in volcanic springs e.g. SABALAN mountain area.

Mahdi Salimi (corresponding author) graduated in electrical engineering from Islamic Azad University (IAU) (Science and Research Branch), Tehran, Iran, in 2012. He worked as an Assistant Professor from 2012 until 2019 at the IAU University, Ardabil Branch, Iran, in the Electrical and Electronics Department. In 2019 he joined the University of Nottingham, Power Electronics, Machine, and Control (PEMC) Group as a Researcher for three years. Since April 2022, he has worked at Greenwich University as a Lecturer of power electronics. He has published 35 papers in peer-reviewed journals and 24 papers published in international conferences. His research areas include design, closed-loop control, simulation, and practical implementation of the power electronics systems for more/full electric aircraft and vehicles, grid-connected renewable energy systems, active power filters, and wireless chargers. (Email: m.salimi@gre.ac.uk)

Seyed Mohammad Taghi Bathaee was born in Iran, in 1950. He received the B.Sc. degree in power engineering from the K. N. Toosi University of Technology, Tehran, Iran, in 1977, the M.S. degree in power engineering from George Washington University, Washington DC, USA, in 1979, and the Ph.D. degree from the Amirkabir University of Technology, Tehran, in 1995. He is currently a Professor and a Member of the Academic Staff of the K. N. Toosi University of Technology. His research interests include renewable energy, smart grid, power system dynamic and control, and power system transient.

Davar Mirabbasi was born in Ardabil, Iran, in 1982. He received the Ph.D. degree in electrical engineering from Shahid Chamran University of Ahwaz, Ahwaz, Iran, in

2014. Since 2006, he has been with the Faculty of Electrical Engineering at Islamic Azad University, Ardabil Branch, Ardabil, Iran, where he is a Professor of Electrical Engineering. His research interests include smart grids, power system planning, and power electronics applications.